Journal of Computational Physics **175,** 108–127 (2002)
doi:10.1006/jcph.2001.6892, available online at http://www.idealibrary.com on IDEAL®

A Technique of Treating Negative Weights in WENO Schemes[1]

Jing Shi, Changqing Hu,[2] and Chi-Wang Shu

Division of Applied Mathematics, Brown University, Providence, Rhode Island 02912
E-mail: shi@cfm.brown.edu; phu@us.oracle.com; shu@cfm.brown.edu

Received November 22, 2000; revised July 10, 2001

High-order accurate weighted essentially nonoscillatory (WENO) schemes have recently been developed for finite difference and finite volume methods both in structured and in unstructured meshes. A key idea in WENO scheme is a linear combination of lower order fluxes or reconstructions to obtain a higher order approximation. The combination coefficients, also called linear weights, are determined by local geometry of the mesh and order of accuracy and may become negative, such as in the central WENO schemes using staggered meshes, high-order finite volume WENO schemes in two space dimensions, and finite difference WENO approximations for second derivatives. WENO procedures cannot be applied directly to obtain a stable scheme if negative linear weights are present. The previous strategy for handling this difficulty is either by regrouping of stencils or by reducing the order of accuracy to get rid of the negative linear weights. In this paper we present a simple and effective technique for handling negative linear weights without a need to get rid of them. Test cases are shown to illustrate the stability and accuracy of this approach.

Key Words: Weighted essentially nonoscillatory; negative weights; stability; high-order accuracy; shock calculation.

1. INTRODUCTION

High-order accurate weighted essentially nonoscillatory (WENO) schemes have recently been developed to solve a hyperbolic conservation law

$$u_t + \nabla \cdot f(u) = 0. \tag{1.1}$$

[1] Research supported by ARO Grants DAAG55-97-1-0318 and DAAD19-00-1-0405, NSF Grants DMS-9804985 and ECS-9906606, NASA Langley Grant NAG-1-2070, and Contract NAS1-97046 while the third author was in residence at ICASE, NASA Langley Research Center, Hampton, VA 23681-2199, and AFOSR Grant F49620-99-1-0077.

[2] Current address: Oracle, 3OP6, 500 Oracle Parkway, Redwood Shores, CA 94065.

0021-9991/02 $35.00

The first WENO scheme was constructed in [19] for a third-order finite volume version in one space dimension. In [10], third- and fifth-order finite difference WENO schemes in multispace dimensions were constructed, with a general framework for the design of the smoothness indicators and nonlinear weights. Later, second-, third-, and fourth-order finite volume WENO schemes for 2D general triangulation were developed [4, 8]. Very high-order finite difference WENO schemes (for orders between 7 and 13) were developed in [1]. Central WENO schemes were developed in [12–14].

WENO schemes are designed based on the successful ENO schemes in [7, 24, 25]. Both ENO and WENO use the idea of adaptive stencils in the reconstruction procedure based on the local smoothness of the numerical solution to automatically achieve high-order accuracy and nonoscillatory property near discontinuities. ENO uses just one (optimal in some sense) out of many candidate stencils when doing the reconstruction; while WENO uses a convex combination of all the candidate stencils, each being assigned a nonlinear weight which depends on the local smoothness of the numerical solution based on that stencil. WENO improves upon ENO in robustness, better smoothness of fluxes, better steady-state convergence, better provable convergence properties, and more efficiency. For a detailed review of ENO and WENO schemes, we refer to the lecture notes [22, 23].

WENO schemes have already been widely used in applications. Some of the examples include dynamical response of a stellar atmosphere to pressure perturbations [3]; shock vortex interactions and other gas dynamics problems [5, 6]; incompressible flow problems [27]; Hamilton–Jacobi equations [9]; magneto-hydrodynamics [11]; underwater blast-wave focusing [15]; the composite schemes and shallow water equations [16, 17]; real gas computations [20]; wave propagation using Fey's method of transport [21]; and so forth.

A key idea in WENO schemes is a linear combination of lower order fluxes or reconstructions to obtain a higher order approximation. The combination coefficients, also called linear weights, are determined by local geometry of the mesh and order of accuracy and may become negative, such as in the central WENO schemes using staggered meshes, by high-order finite volume WENO schemes in two space dimensions, and by finite difference WENO approximations for second derivatives. WENO procedures cannot be applied directly to obtain a stable scheme if negative linear weights are present. The previous strategy for handling this difficulty is either by regrouping of stencils (e.g., in [8]) or by reducing the order of accuracy (e.g., in [12]) to get rid of the negative linear weights. In this paper, we present a simple and effective technique for handling negative linear weights without a need to get rid of them. Test cases will be shown to illustrate the stability and accuracy of this approach.

We first summarize the general WENO reconstruction procedure, consisting of the following steps. We assume we have a given cell $\triangle$ (which could be an interval in 1D, a rectangle in a 2D tensor product mesh, or a triangle in a 2D unstructured mesh) and a fixed point x^G within or on one edge of the cell.

1. We identify several stencils $\mathcal{S}_j$, $j = 1, \ldots, q$, such that $\triangle$ belongs to each stencil. We denote by $\mathcal{T} = \bigcup_{j=1}^{q} \mathcal{S}_j$ the larger stencil which contains all the cells from the q smaller stencils.

2. We have a (relatively) lower order reconstruction or interpolation function (usually a polynomial), denoted by $p_j(x)$, associated with each of the stencils $\mathcal{S}_j$, for $j = 1, \ldots, q$. We also have a (relatively) higher order reconstruction or interpolation function (again usually a polynomial), denoted by $Q(x)$, associated with the larger stencil $\mathcal{T}$.

3. We find the combination coefficients, also called linear weights, denoted by $\gamma_1, \ldots, \gamma_q$, such that

$$Q(x^G) = \sum_{j=1}^{q} \gamma_j p_j(x^G) \tag{1.2}$$

for all possible given data in the stencils. These linear weights depend on the mesh geometry, the point x^G, and the specific reconstruction or interpolation requirements, but *not* on the given solution data in the stencils.

4. We compute the smoothness indicator, denoted by β_j, for each stencil $\mathcal{S}_j$, which measures how smooth the function $p_j(x)$ is in the target cell $\triangle$. The smaller this smoothness indicator β_j, the smoother the function $p_j(x)$ is in the target cell. In all of the current WENO schemes, we are using the smoothness indicator

$$\beta_j = \sum_{1 \le |\alpha| \le k} \int_{\triangle} |\triangle|^{2|\alpha|-1} (D^\alpha p_j(x))^2 \, dx \tag{1.3}$$

for $j = 1, \ldots, q$, where k is the degree of the polynomial $p_j(x)$, $|\triangle|$ is the length of the cell $\triangle$ in 1D, and $D^\alpha = \partial_{x_1}^{\alpha_1} \partial_{x_2}^{\alpha_2} \cdots \partial_{x_d}^{\alpha_d}$ and $|\alpha| = \alpha_1 + \alpha_2 + \cdots + \alpha_d$ for the multi-index $\alpha = (\alpha_1, \alpha_2, \ldots, \alpha_d)$ in d space dimensions. The factor $|\triangle|^{2|\alpha|-1}$ is different for 2D or 3D: If $|\triangle|$ denotes the area of the cell $\triangle$ in 2D and the volume of the cell $\triangle$ in 3D, then the factors are $|\triangle|^{|\alpha|-1}$ in 2D and $|\triangle|^{\frac{2}{3}|\alpha|-1}$ in 3D, respectively. The purpose of this factor is to bring the smoothness indicator invariant under spatial scaling.

5. We compute the nonlinear weights based on the smoothness indicators

$$\omega_j = \frac{\tilde{\omega}_j}{\sum_j \tilde{\omega}_j}, \quad \tilde{\omega}_j = \frac{\gamma_j}{(\varepsilon + \beta_j)^2}, \tag{1.4}$$

where γ_j are the linear weights determined in step 3 above, and ε is a small number to avoid the denominator to become 0. We are using $\varepsilon = 10^{-6}$ in all the computations in this paper. The final WENO approximation or reconstruction is then given by

$$R(x^G) = \sum_{j=1}^{q} \omega_j p_j(x^G). \tag{1.5}$$

We remark that all the coefficients in the above steps which depend on the mesh but not on the data of the numerical solution, such as γ_j in (1.2), the linear coefficients in the reconstructions $p_j(x)$ in step 2, and the quadratic coefficients in the smoothness indicators β_j in (1.3), should be computed and stored at the beginning of the code after the generation of the mesh but before the time evolution starts.

We now use a simple example to illustrate the steps outlined above. We assume we are given a uniform mesh $I_i = (x_{i-1/2}, x_{i+1/2})$ and cell averages of a function $u(x)$ in these cells, denoted by $\overline{u}_i$. We would like to find a fifth-order WENO reconstruction to the point value $u(x_{i+1/2})$, based on a stencil of five cells $\{I_{i-2}, I_{i-1}, I_i, I_{i+1} I_{i+2}\}$, with the target cell containing the point $x_{i+1/2}$ chosen as $\triangle = I_i$.

In step 1 above, we could have the three stencils

$$\mathcal{S}_1 = \{I_{i-2}, I_{i-1}, I_i\}, \qquad \mathcal{S}_2 = \{I_{i-1}, I_i, I_{i+1}\}, \qquad \mathcal{S}_3 = \{I_i, I_{i+1}, I_{i+2}\},$$

which make up a larger stencil

$$\mathcal{T} = \{I_{i-2}, I_{i-1}, I_i, I_{i+1}, I_{i+2}\}. \tag{1.6}$$

In step 2 above we would have three polynomials $p_j(x)$ of degree of at most two, with their cell averages agreeing with that of the function u in the three cells in each stencil $\mathcal{S}_j$. The higher order function $Q(x)$ is a polynomial of degree of at most four, with its cell averages agreeing with that of the function u in the five cells in the larger stencil $\mathcal{T}$. The three lower order approximations to $u(x_{i+1/2})$, associated with $p_j(x)$, in terms of the given cell averages of u, are given by

$$\begin{aligned} p_1\big(x_{i+1/2}\big) &= \frac{1}{3}\bar{u}_{i-2} - \frac{7}{6}\bar{u}_{i-1} + \frac{11}{6}\bar{u}_i, \\ p_2\big(x_{i+1/2}\big) &= -\frac{1}{6}\bar{u}_{i-1} + \frac{5}{6}\bar{u}_i + \frac{1}{3}\bar{u}_{i+1}, \\ p_3\big(x_{i+1/2}\big) &= \frac{1}{3}\bar{u}_i + \frac{5}{6}\bar{u}_{i+1} - \frac{1}{6}\bar{u}_{i+2}. \end{aligned} \tag{1.7}$$

The coefficients in front of the $\bar{u}$ could be derived by Lagrange polynomials or by solving a small 3×3 linear system, from the condition that the quadratic polynomial $p_j(x)$ has the same cell averages as the given $\bar{u}$ in the relevant stencil. See [22] for details. Each of the $p_j(x_{i+1/2})$ in (1.7) is a third-order approximation to $u(x_{i+1/2})$. The higher order approximation to $u(x_{i+1/2})$, associated with $Q(x)$, is given by

$$Q(x_{i+1/2}) = \frac{1}{30}\bar{u}_{i-2} - \frac{13}{60}\bar{u}_{i-1} + \frac{47}{60}\bar{u}_i + \frac{9}{20}\bar{u}_{i+1} - \frac{1}{20}\bar{u}_{i+2}, \tag{1.8}$$

which is a fifth-order approximation to $u(x_{i+1/2})$.

In step 3 above, we would have

$$\gamma_1 = \frac{1}{10}, \qquad \gamma_2 = \frac{3}{5}, \qquad \gamma_3 = \frac{3}{10}. \tag{1.9}$$

It can be readily verified, using (1.7) and (1.8), that

$$Q\big(x_{i+1/2}\big) = \gamma_1 p_1\big(x_{i+1/2}\big) + \gamma_2 p_2\big(x_{i+1/2}\big) + \gamma_3 p_3\big(x_{i+1/2}\big)$$

for all possible given data $\bar{u}_j$, $j = i-2, i-1, i, i+1, i+2$.

In step 4 above, we could easily work out from (1.3) the three smoothness indicators given by

$$\begin{aligned} \beta_1 &= \frac{13}{12}(\bar{u}_{i-2} - 2\bar{u}_{i-1} + \bar{u}_i)^2 + \frac{1}{4}(\bar{u}_{i-2} - 4\bar{u}_{i-1} + 3\bar{u}_i)^2 \\ \beta_2 &= \frac{13}{12}(\bar{u}_{i-1} - 2\bar{u}_i + \bar{u}_{i+1})^2 + \frac{1}{4}(\bar{u}_{i-1} - \bar{u}_{i+1})^2 \\ \beta_3 &= \frac{13}{12}(\bar{u}_i - 2\bar{u}_{i+1} + \bar{u}_{i+2})^2 + \frac{1}{4}(3\bar{u}_i - 4\bar{u}_{i+1} + \bar{u}_{i+2})^2. \end{aligned} \tag{1.10}$$

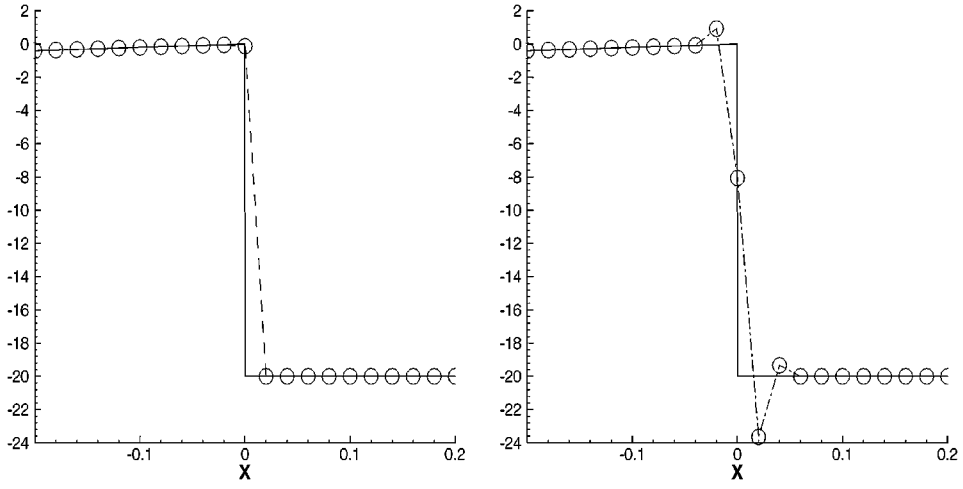

FIG. 1.1. Reconstructions to $u(x_{i+1/2})$. Solid lines: exact function; symbols: numerical approximations. Left: fifth-order WENO. Right: fifth-order traditional.

We notice in particular that the linear weights $\gamma_1, \gamma_2, \gamma_3$ in step 3 above are all positive. In such cases, the WENO reconstruction procedure outlined above and the scheme based on it work very well. In Fig. 1.1, we plot the approximation to $u(x)$ for a discontinuous function $u(x) = 2x$ for $x \le 0$ and $u(x) = -20$ otherwise, by the fifth-order WENO reconstruction on the left and by the fifth-order traditional reconstruction (1.8) on the right, with a mesh $x_i = (i - 0.4965)\Delta x$ with $\Delta x = 0.02$. We can clearly see that WENO avoids the overshoots and undershoots near the discontinuity.

We now look at another simple example in which some of the linear weights in step 3 above would become negative. We have exactly the same setting as above except that now we seek the reconstruction not at the cell boundary but at the cell center x_i. This is needed by the central schemes with staggered grids [12]. Thus, step 1 would stay the same as above; step 2 would produce

$$\begin{aligned} p_1(x_i) &= -\frac{1}{24}\bar{u}_{i-2} + \frac{1}{12}\bar{u}_{i-1} + \frac{23}{24}\bar{u}_i, \\ p_2(x_i) &= -\frac{1}{24}\bar{u}_{i-1} + \frac{13}{12}\bar{u}_i - \frac{1}{24}\bar{u}_{i+1}, \\ p_3(x_i) &= \frac{23}{24}\bar{u}_i + \frac{1}{12}\bar{u}_{i+1} - \frac{1}{24}\bar{u}_{i+2}. \end{aligned} \tag{1.11}$$

Each of these steps is a third-order reconstruction to $u(x_i)$. The higher order reconstruction to $u(x_i)$, associated with $Q(x)$, is given by

$$Q(x_i) = \frac{3}{640}\bar{u}_{i-2} - \frac{29}{480}\bar{u}_{i-1} + \frac{1067}{960}\bar{u}_i - \frac{29}{480}\bar{u}_{i+1} + \frac{3}{640}\bar{u}_{i+2}, \tag{1.12}$$

which is a fifth-order reconstruction to $u(x_i)$. Step 3 would produce the following weights:

$$\gamma_1 = -\frac{9}{80}, \qquad \gamma_2 = \frac{49}{40}, \qquad \gamma_3 = -\frac{9}{80}.$$

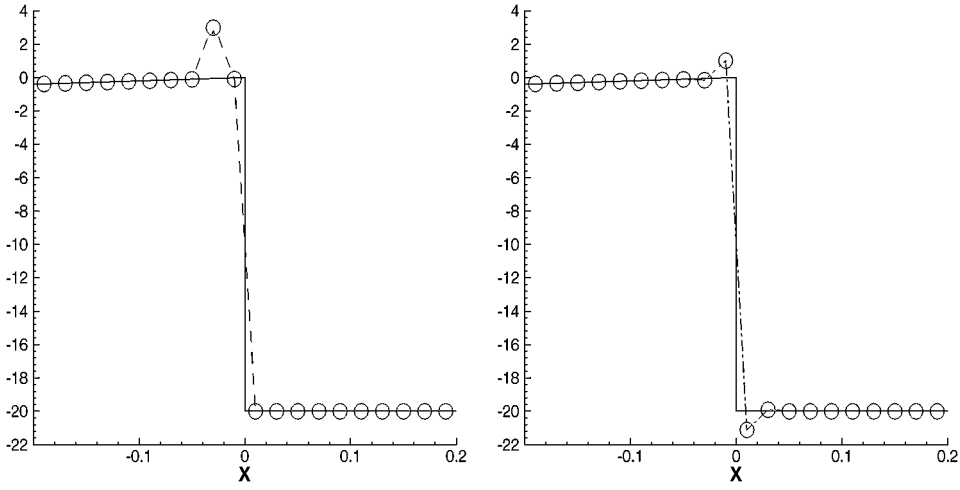

FIG. 1.2. Reconstructions to $u(x_i)$. Solid lines: exact function; symbols: numerical approximations. Left: fifth-order WENO. Right: fifth-order traditional.

Notice that two of them are negative. The smoothness indicators in step 4 will remain the same. This time, the WENO approximation, shown at the left of Fig. 1.2, is less satisfactory (in fact, even worse than a traditional fifth-order reconstruction shown on the right), because of the negative linear weights.

We remark that negative linear weights do not appear in finite difference WENO schemes in any spatial dimensions for conservation laws for any order of accuracy [1, 10], and they do not appear in one-dimensional as well as some multidimensional finite volume WENO schemes for conservation laws. Unfortunately, they do appear in some other cases, such as the central WENO schemes using staggered meshes we have seen above, high-order finite volume schemes for two dimensions described in [8] and in this paper, and finite difference WENO approximations for second derivatives.

Although the details of WENO schemes applied to the conservation law (1.1) can be found in the literature, e.g., [10, 22, 23], we still include a brief summary of all the steps of a WENO finite volume scheme applied to (1.1) in the one-dimensional scalar case for the positive wind case $f'(u) \geq 0$, for completeness. The algorithm consists of the following steps:

1. Given the cell averages $\bar{u}_i$ for all cells I_i for time level n (starting from time level 0 which is the initial condition);

2. Reconstruct the point values $u^-_{i+1/2}$ for all cell boundaries $x_{i+1/2}$ using the reconstruction procedure detailed above. That is, we use (1.5) with ω_j defined by (1.4), using γ_j given by (1.9) and β_j given by (1.10). The superscript "$-$" in $u^-_{i+1/2}$ refers to the fact that the reconstruction has a stencil (1.6) biased to the left relative to the location $x_{i+1/2}$. This is upwinding according to the wind direction $f'(u) \geq 0$.

3. Form the residue for time level n in the method-of-lines ODE

$$\frac{d\bar{u}_i}{dt} = \frac{1}{\Delta x}\left(f\left(u^-_{i+1/2}\right) - f\left(u^-_{i-1/2}\right)\right),$$

and move to time level $n+1$ by a high-order TVD Runge–Kutta method [24].

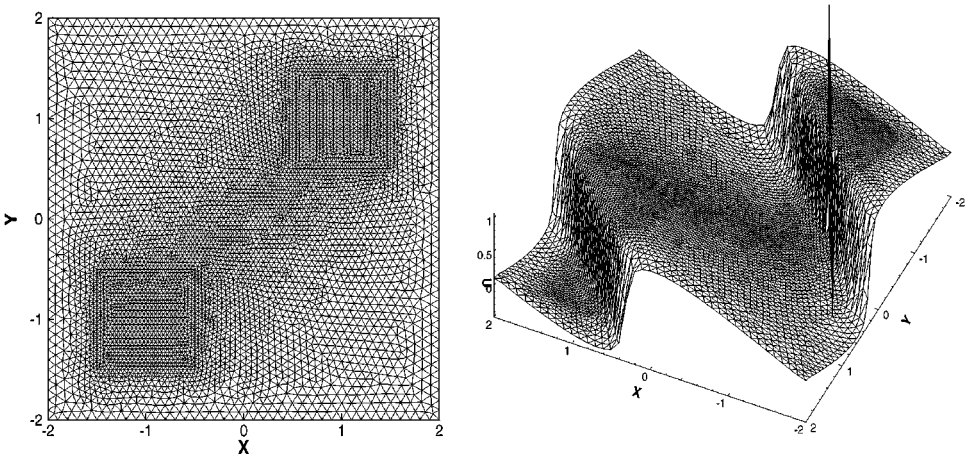

FIG. 1.3. 2D Burgers' equation. Left: nonuniform triangular mesh used in the computation. Right: fourth-order WENO result at $t = 0.473$, CFL $= 0.2$, without any special treatment for the negative linear weights.

If $f'(u)$ could change sign, then both $u^-_{i+1/2}$ and $u^+_{i+1/2}$, which has a stencil biased to the right, must be computed in the second step, and a monotone flux (an approximate Riemann solver in the system case) $\hat{f}(u^-_{i+1/2}, u^+_{i+1/2})$ would replace $f(u^-_{i+1/2})$ in the third step. For details, see, e.g., [10, 22, 23].

For all the calculations reported in this paper, we have taken a CFL number equal to 0.6 for the rectangular codes and 0.5 for the triangular codes, unless otherwise indicated. Usually, WENO schemes with third-order TVD Runge–Kutta methods [24] are stable for CFL numbers below 0.8 for the structured mesh, and below 0.6 for the triangular mesh.

While on approximation alone the appearance of negative linear weights might be annoying but perhaps not fatal (Fig. 1.2); in solving a PDE, the result might be more serious. As an example, in Fig. 1.3 we show the results of using a fourth-order finite volume WENO scheme [8] on a nonuniform triangular mesh shown at the left, which has been chosen to yield significant negative linear weights, for solving the two-dimensional Burgers equation,

$$u_t + \left(\frac{u^2}{2}\right)_x + \left(\frac{u^2}{2}\right)_y = 0, \tag{1.13}$$

in the domain $[-2, 2] \times [-2, 2]$ with an initial condition $u_0(x, y) = 0.3 + 0.7 \sin(\frac{\pi}{2}(x + y))$ and periodic boundary conditions. We can see that serious oscillation appears at the point $(-1.08, -0.67)$ near the shock in the numerical solution once the shock has developed. The oscillation eventually leads to instability and blowing up of the numerical solution for this example. In fact, in all the test cases involving negative linear weights and discontinuous solutions presented in this paper, WENO schemes without special treatment to the negative weights are unstable (the numerical solution blows up and the code stops). The figures of such unstable cases are similar to Fig. 1.3 and hence are not shown.

The main purpose of this paper is to develop a simple and effective technique for handling negative linear weights without a need to get rid of them. Test cases will be shown to illustrate the stability and accuracy of this approach.

2. A SPLITTING TECHNIQUE

We now introduce a splitting technique to treat the negative weights. It is very simple, involves little additional cost, yet is quite effective. The WENO procedure outlined in the previous section is only modified in step 5 in the following way:

5′ If $\min(\gamma_1, \ldots, \gamma_q) \geq 0$ proceed as before. Otherwise, we split the linear weights into two parts: positive and negative. Define

$$\tilde{\gamma}_i^+ = \frac{1}{2}(\gamma_i + \theta|\gamma_i|), \qquad \tilde{\gamma}_i^- = \tilde{\gamma}_i^+ - \gamma_i, \qquad i = 1, \ldots, q \tag{2.1}$$

where we take $\theta = 3$ in all the numerical tests. We then scale them by

$$\sigma^\pm = \sum_{j=1}^{q} \tilde{\gamma}_j^\pm; \qquad \gamma_i^\pm = \tilde{\gamma}_i^\pm / \sigma^\pm, \qquad i = 1, \ldots, q. \tag{2.2}$$

We now have two split polynomials

$$Q^\pm(x^G) = \sum_{j=1}^{q} \gamma_j^\pm p_j(x^G), \tag{2.3}$$

which satisfy

$$Q(x^G) = \sigma^+ Q^+(x^G) - \sigma^- Q^-(x^G). \tag{2.4}$$

We can then define the nonlinear weights (1.4) for the positive and negative groups $\gamma_j^\pm$ separately, denoted by $\omega_j^\pm$, based on the same smoothness indicator β_j. We will then define the WENO approximation $R^\pm(x^G)$ separately by (1.5), using $\omega_j^\pm$, and form the final WENO approximation by

$$R(x^G) = \sigma^+ R^+(x^G) - \sigma^- R^-(x^G).$$

We remark that the key idea of this decomposition is to make sure that every stencil has a significant representation in both the positive and the negative weight groups. Within each group, the WENO idea of redistributing the weights subject to a fixed sum according to the smoothness of the approximation is still followed as before. While in the unsplit case, the nonlinear weights may become extremely large or small in magnitudes because of the lack of convexity, the split positive and negative nonlinear weights stay bounded as they separately sum to fixed constants of the linear weights. Moreover, it is expected that the distribution of the magnitudes of nonlinear weights in each of the positive and negative group follows the smoothness of the solution, as every stencil has its "fair share" in each of the positive and negative linear weight groups. We have performed extensive numerical experiments about many plausible approaches of splitting, and those used here have been found to be the most robust.

For the simple example of fifth-order WENO reconstruction to $u(x_i)$, the split linear weights corresponding to (2.1) are, before the scaling,

$$\tilde{\gamma}_1^+ = \frac{9}{80}, \quad \tilde{\gamma}_1^- = \frac{9}{40}, \qquad \tilde{\gamma}_2^+ = \frac{49}{20}, \quad \tilde{\gamma}_2^- = \frac{49}{40}, \qquad \tilde{\gamma}_3^+ = \frac{9}{80}, \quad \tilde{\gamma}_3^- = \frac{9}{40}.$$

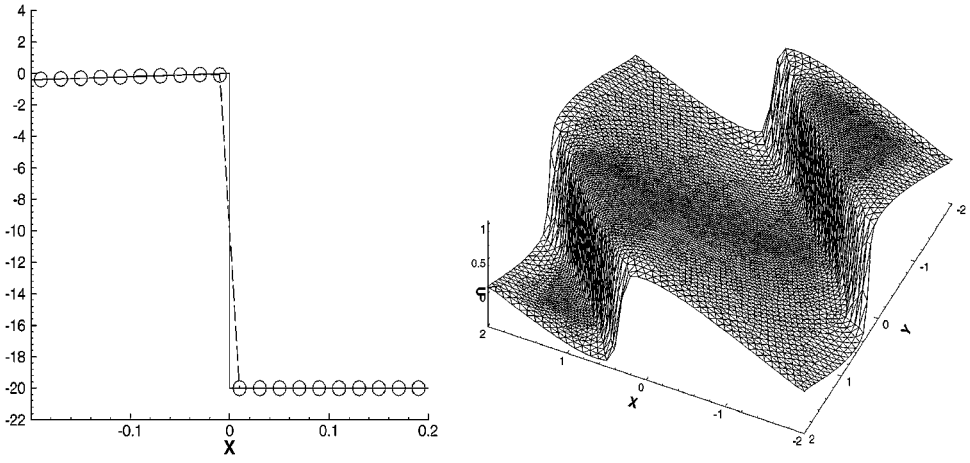

FIG. 2.1. WENO approximations with the splitting treatment for negative linear weights. Left: approximation to $u(x_i)$. Right: Burgers equation, solution at $t = 5/\pi^2$, CFL $= 0.2$.

We notice that, as the most expensive part of the WENO procedure, namely the computation of the smoothness indicators (1.3), has not changed, the extra cost of this positive/negative weight splitting is very small.

However, this simple and inexpensive change makes a big difference to the computations. In Fig. 2.1, we show the result of the two previous unsatisfactory cases—the fifth-order WENO reconstruction to $u(x_i)$ in Fig. 1.2 left, and the approximation to the Burgers equation in Fig. 1.3 right—now using WENO schemes with this splitting treatment. We can see clearly that the results are now as good as one would get from WENO schemes having only positive linear weights.

It is easy to prove that the splitting maintains the accuracy of the approximation in smooth regions. We will demonstrate this fact in the following sections. We will also demonstrate the effectiveness of this simple splitting technique through a few selected numerical examples in the next sections. The main WENO schemes we will consider are fifth-order finite volume WENO schemes on Cartesian meshes, and the third- and fourth-order finite volume WENO schemes on triangular meshes. In both cases, negative linear weights appear regularly.

The calculations are performed on SUN Ultra workstations and also on the IBM SP parallel computer at TCASCV of Brown University. The parallel efficiency of the method is excellent (more than 90%).

3. 2D FINITE VOLUME WENO SCHEMES ON CARTESIAN MESHES

3.1. The Schemes

We describe two different ways to construct fifth-order finite volume WENO schemes on Cartesian meshes. Compared with finite difference WENO methods [10], finite volume methods have the advantage of an applicability of using arbitrary nonuniform meshes, at the price of increased computational cost [2].

We define the cell

$$I_{i,j} \equiv \left[x_{i-\frac{1}{2}}, x_{i+\frac{1}{2}}\right] \times \left[y_{j-\frac{1}{2}}, y_{j+\frac{1}{2}}\right] \tag{3.1}$$

for $i = 1, \ldots, m$, $j = 1, \ldots, n$, where $I_{i,j}$ needs not be uniform or smooth varying.

The three-point Gaussian quadrature rule is used at each cell edge when evaluating the numerical flux in order to maintain fifth-order accuracy. Let (x^G, y^G) denote one of the Gaussian quadrature points at the cell boundary of $I_{i,j}$ given by $\Gamma \equiv \{x = x_{i-\frac{1}{2}}, y_{j-\frac{1}{2}} \le y \le y_{j+\frac{1}{2}}\}$. There are two ways to perform a WENO reconstruction at the point (x^G, y^G).

Genuine 2D

The first WENO reconstruction is genuine 2D finite volume using 5×5 cells. We can see that there are a total of nine stencils $\mathcal{S}_{s,t}(s, t = -1, 0, 1)$. Each stencil $\mathcal{S}_{s,t}$ contains 3×3 cells centered around $I_{i+s,j+t}$. On each stencil we can construct a Q^2 polynomial (tensor product of second-order polynomials in x and y) satisfying the cell average condition (i.e., its cell average in each cell inside the stencil equals to the given value). Let

$$\mathcal{T} = \bigcup_{s,t=-1}^{1} \mathcal{S}_{s,t},$$

which contains 5×5 cells centered around $I_{i,j}$. On $\mathcal{T}$ we can construct a Q^4 polynomial satisfying the cell average condition. The WENO reconstruction is then performed according to the steps outlined in Sections 1 and 2.

We now make the following remarks:

1. By using a Lagrange interpolation basis, we can easily find the unique linear weights.
2. Even for a uniform mesh, a negative linear weight appears for the middle Gaussian point $(x^G, y^G) = (x_{i-\frac{1}{2}}, y_j)$. Such an appearance of negative linear weights has also been observed in the central WENO schemes [12]; see the examples in Sections 1 and 2.
3. By Taylor expansions, we can prove that the smoothness indicators yield a uniform fifth-order accuracy in smooth regions. See [10] for the method of proof.

Dimension by Dimension

The second WENO reconstruction exploits the tensor product nature of the interpolation we use. This WENO procedure is performed in a dimension by dimension fashion. The WENO schemes applied in [5, 6] belong to this class. Consider the point (x^G, y^G) as above. First, we perform a one-dimensional WENO reconstruction in the y-direction, in order to get the one-dimensional cell averages (in the x-direction) $w(\bullet, y^G)$. Then we perform another one-dimensional WENO reconstruction to w in the x-direction, to obtain the final reconstructed point value at (x^G, y^G).

We make the following remarks:

1. For a scalar equation, the underlying linear reconstructions of the above two versions are equivalent. For nonlinear WENO reconstructions, they are not equivalent. Both of them are fifth-order accurate but the actual errors on the same mesh may be different; see Table 3.1 below.
2. For systems of conservation laws, such as the Euler equations of gas dynamics, both versions of the WENO reconstruction should be performed in local characteristic fields, for genuinely high-order (order 5 in this paper) versions. For lower order schemes, especially with a centered formulation [12] but also with some upwind versions [18], the reconstruction can be performed directly on each component.

TABLE 3.1
2D Vortex Evolution

		Genuine FV		Dim-by-dim	
N	Δx	L^∞ error	Order	L^∞ error	Order
20	6.71E-1	4.38E-2		5.26E-2	
40	3.77E-1	3.10E-3	4.59	5.66E-3	3.86
80	2.01E-1	1.20E-4	5.15	3.96E-4	4.22
160	1.00E-1	4.39E-6	4.76	7.96E-6	5.62
320	5.00E-2	1.88E-7	4.53	2.90E-7	4.77

3. The dimension by dimension version of the WENO reconstruction is less expensive and requires smaller memory than the genuine two-dimensional version. The CPU time saving is about a factor of 4 for the Euler equations in our implementation. The computed results are mostly similar from both versions.

In the following, we will give numerical examples computed by the above WENO schemes. The splitting technique has been used in all the computations when negative linear weights appear. We will show the results for both smooth and discontinuous problems.

3.2. 2D Vortex Evolution

First, we check the accuracy of the WENO schemes constructed above. The two-dimensional vortex evolution problem [8, 22] is used as a test problem.

We solve the Euler equations for compressible flow in 2D

$$U_t + f(U)_x + g(U)_y = 0, \tag{3.2}$$

where

$$\begin{aligned} U &= (\rho, \rho u, \rho v, E)^T, \\ f(U) &= (\rho u, \rho u^2 + p, \rho uv, u(E + p))^T, \\ g(U) &= (\rho v, \rho uv, \rho v^2 + p, v(E + p))^T. \end{aligned}$$

Here ρ is the density, (u, v) is the velocity, E is the total energy, p is the pressure, related to the total energy by $E = \frac{p}{\gamma - 1} + \frac{1}{2}\rho(u^2 + v^2)$ with $\gamma = 1.4$.

The setup of the problem is as follows: The mean flow is $\rho = 1$, $p = 1$, $(u, v) = (1, 1)$, and the computational domain is $[0, 10] \times [0, 10]$. We add, to the mean flow, an isentropic vortex (perturbations in (u, v) and the temperature $T = \frac{p}{\rho}$, no perturbation in the entropy $S = \frac{p}{\rho^\gamma}$),

$$(\delta u, \delta v) = \frac{\epsilon}{2\pi} e^{0.5(1-r^2)}(-\bar{y}, \bar{x}), \qquad \delta T = -\frac{(\gamma - 1)\epsilon^2}{8\gamma\pi^2} e^{1-r^2}, \qquad \delta S = 0,$$

where $(\bar{x}, \bar{y}) = (x - 5, y - 5)$, $r^2 = \bar{x}^2 + \bar{y}^2$, and the vortex strength $\epsilon = 5$.

We use nonuniform meshes which are obtained by an independent random shifting of each point from a uniform mesh in each direction within 30% of the mesh sizes. The solution is computed up to $t = 2$. Table 3.1 shows the L^∞ errors of ρ. We can see that both the genuine two-dimensional finite volume WENO scheme and the dimension by dimension finite volume WENO scheme can achieve the desired order of accuracy while the genuine two-dimensional scheme gives smaller errors for the same mesh.

3.3. Oblique Shock Tubes

The purpose of this test is to see the capability of the rectangular WENO schemes in resolving waves that are oblique to the computational meshes. For details of the problem, we refer to [10]. The 2D Sod's shock tube problem is solved where the initial jump makes an angle θ against the x axis. We take our computational domain to be $[0, 6] \times [0, 1]$ and the initial jump starting at $(x, y) = (2.25, 0)$ and making a $\theta = \frac{\pi}{4}$ angle with the x axis. The solution is computed up to $t = 1.2$ on a 96×16 uniform mesh. In Fig. 3.1 we plot the density contours computed by the above two WENO schemes and the density cut at the bottom of the computational domain. We can see that both schemes perform equally well in resolving the waves. The genuine two-dimensional scheme gives a slightly better resolution in the contact discontinuity and the rarefaction wave.

3.4. A Mach 3 Wind Tunnel with a Step

This model problem is originally from [26]. The setup of the problem is as follows: The wind tunnel is 1 length unit wide and 3 length units long. The step is 0.2 length units high and is located 0.6 length units from the left-hand end of the tunnel. The problem is initialized by a right-going Mach 3 flow. Reflective boundary conditions are applied along the wall of the tunnel, and inflow/outflow boundary conditions are applied at the entrance/exit. The corner of the step is a singular point, and we treat it the same way as in [26], which is based on the assumption of a nearly steady flow in the region near the corner. We show the density contours at time $t = 4$ in Fig. 3.2. Only the results from the dimension by dimension WENO scheme are shown. Uniform meshes of $\Delta x = \Delta y = \frac{1}{40}, \frac{1}{80}, \frac{1}{160}, \frac{1}{320}$ are used.

3.5. Double Mach Reflection

This problem is also originally from [26]. The computational domain for this problem is chosen to be $[0, 4] \times [0, 1]$. The reflecting wall lies at the bottom, starting from $x = \frac{1}{6}$. Initially a right-moving Mach 10 shock is positioned at $x = \frac{1}{6}$, $y = 0$ and makes a 60° angle with the x axis. For the bottom boundary, the exact postshock condition is imposed for the part from $x = 0$ to $x = \frac{1}{6}$, and a reflective boundary condition is used for the rest. At the top boundary, the flow values are set to describe the exact motion of a Mach 10 shock. We compute the solution up to $t = 0.2$. Figures 3.3 and 3.4 show the equally spaced 30 density contours from 1.5 to 22.7 computed by the genuine two-dimensional and the dimension by dimension WENO schemes. We use uniform meshes with $\Delta x = \Delta y = \frac{1}{240}, \frac{1}{480}$. We can see that the results from both schemes are comparable.

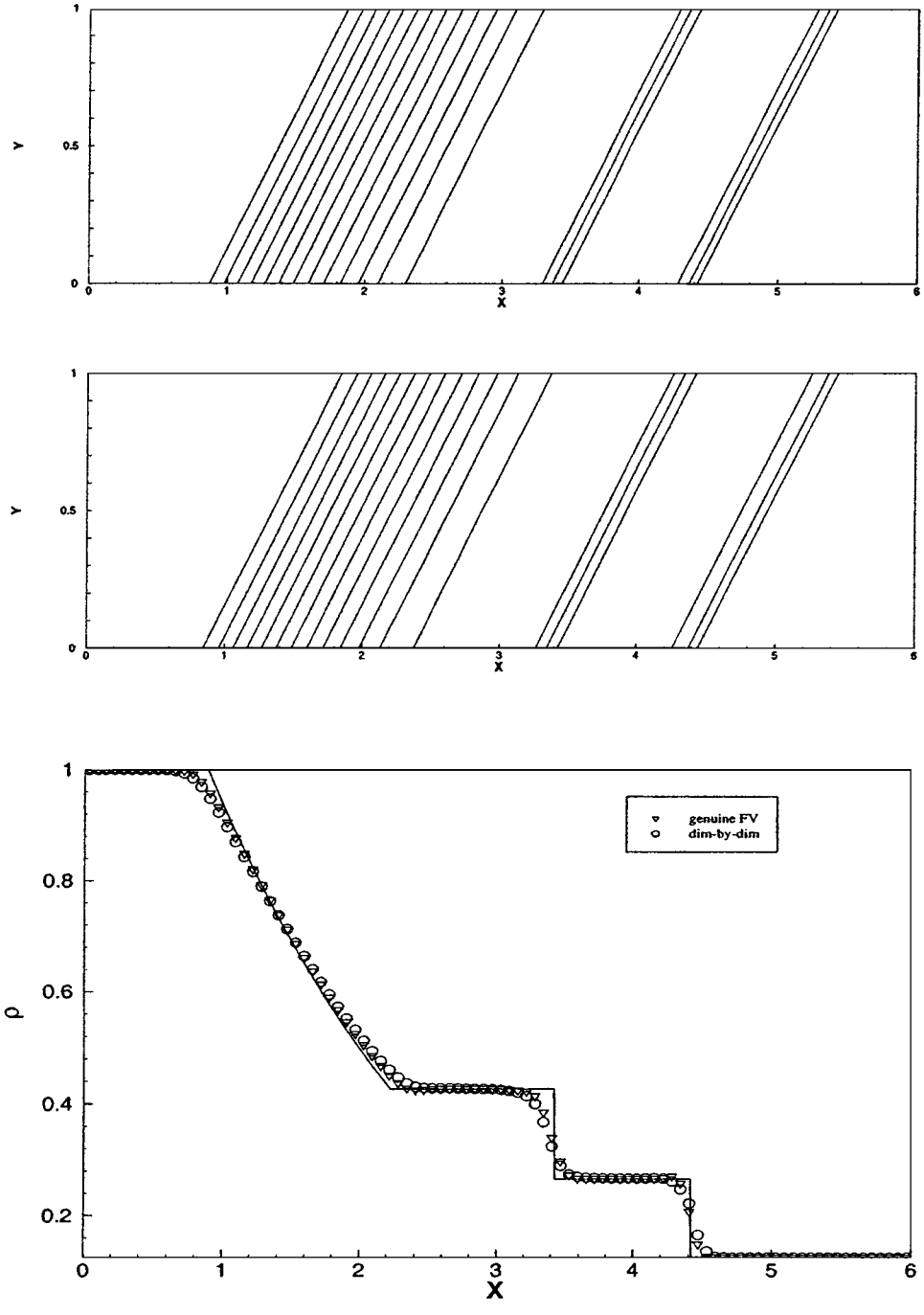

FIG. 3.1. Oblique Sod's problem. Density ρ. Top: contour, genuine two-dimensional WENO; middle: contour, dimension by dimension WENO; bottom: cut at the bottom of the computational domain, the solid line is the exact solution, the triangles are the genuine two-dimensional WENO results, and the circles are the dimension by dimension WENO results.

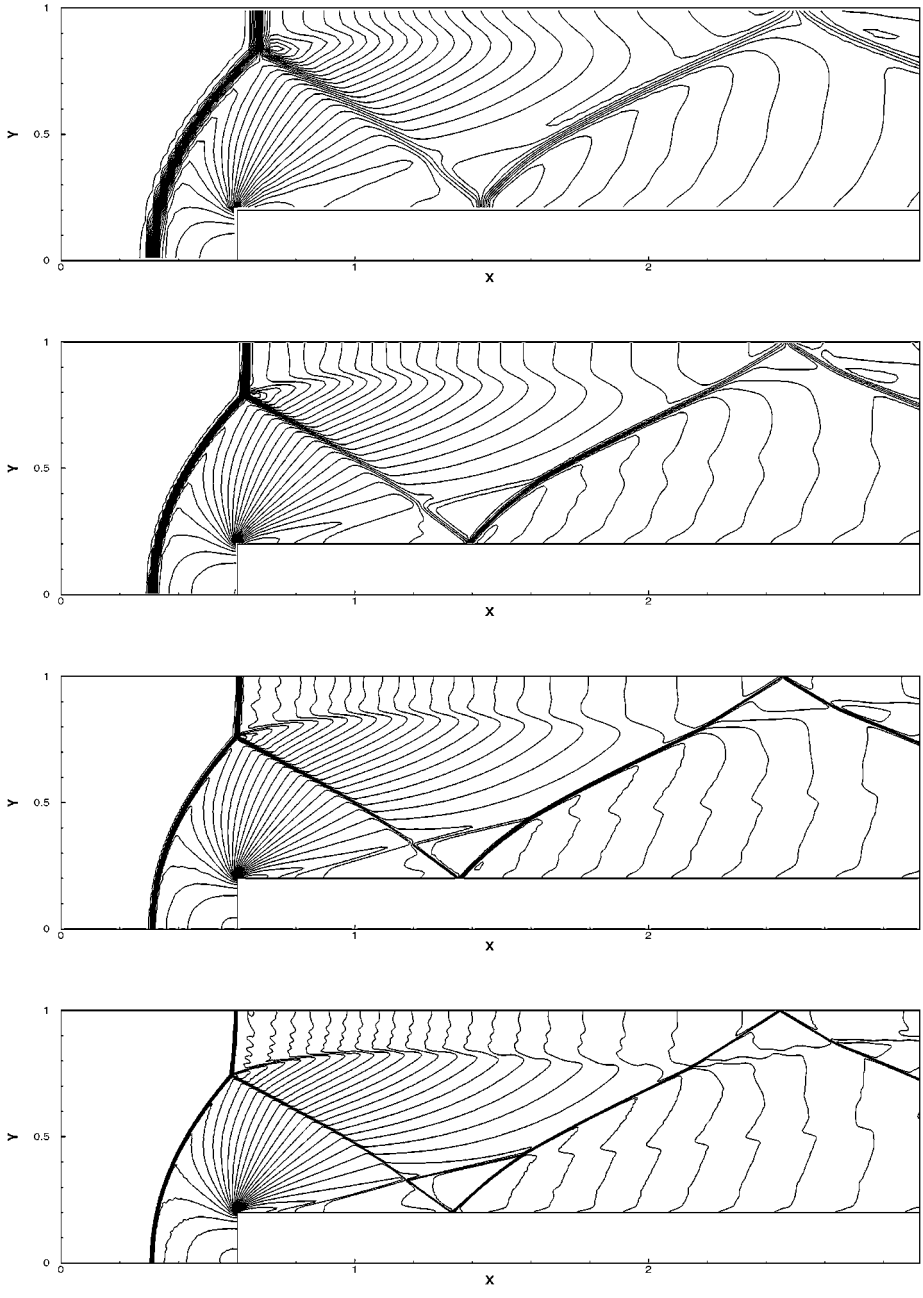

FIG. 3.2. Forward step problem, $\Delta x = \Delta y = \frac{1}{40}, \frac{1}{80}, \frac{1}{160}, \frac{1}{320}$ from top to bottom. Thirty contours from 0.12 to 6.41, dimension by dimension WENO.

4. 2D FINITE VOLUME WENO SCHEMES ON TRIANGULAR MESHES

Both third- and fourth-order finite volume WENO schemes on triangular meshes have been constructed in [8]. The optional linear weights in such schemes are not unique. These are then chosen to avoid negative weights whenever possible, and if that fails, a grouping (of stencils) technique is used in [8], which works fairly well in the third-order case with

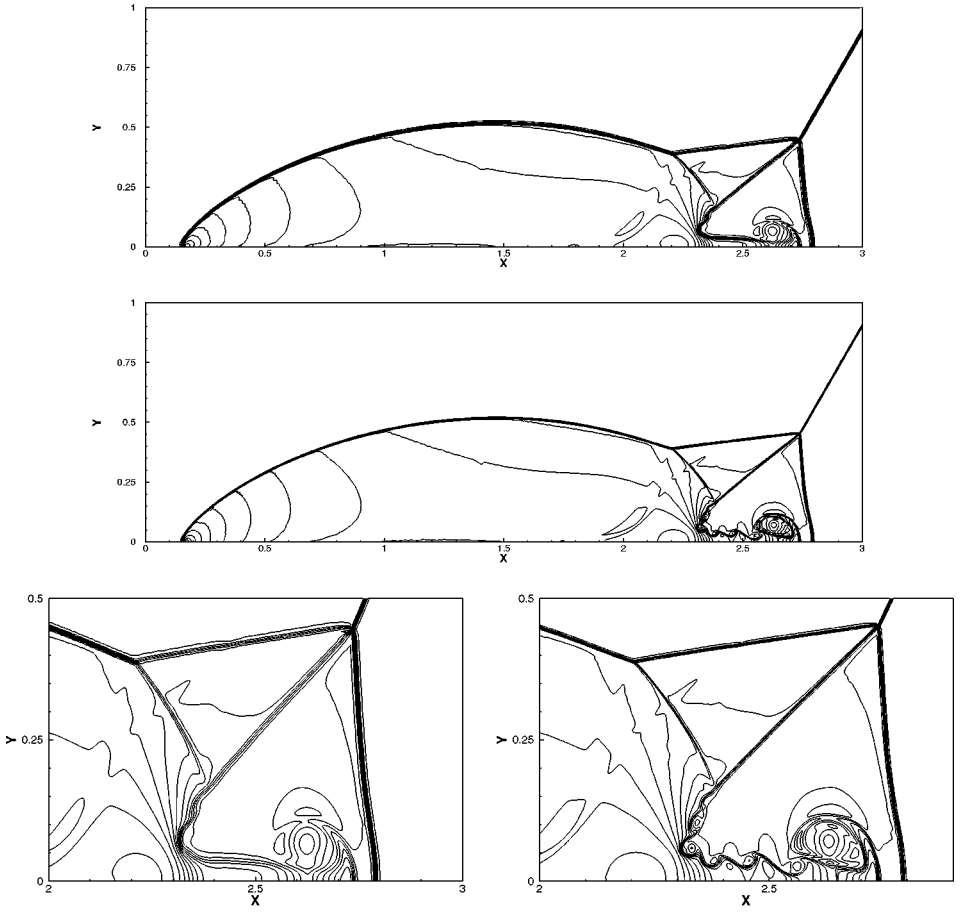

FIG. 3.3. Double Mach reflection, $\Delta x = \Delta y = \frac{1}{240}$ (top and lower left) and $\frac{1}{480}$ (middle and lower right). Genuine two-dimensional WENO. Blow-up regions at the bottom for details.

quite general triangulation but can yield positive weights for the fourth-order case only with fairly uniform triangulation. In this section, we do not seek positive linear weights as in [8], but rather use the splitting technique to treat the negative linear weights when they appear. For scalar equations, the scheme is stable in all runs. For systems of conservation laws, there are still occasional cases of overshoot and instability; the reason seems to be related to characteristic decompositions and is still being investigated.

4.1. Accuracy Check for a Smooth Problem

We solve the 2D Burgers equation (1.13) with the same initial and boundary conditions as before using the fourth-order finite volume WENO scheme [8]. The solution is computed up to $t = \frac{0.5}{\pi^2}$ when no shock has appeared. The meshes used are (1) uniform meshes with equilateral triangulation and (2) random triangulation. For the uniform meshes we do not seek positive weights as was done in [8], rather we use the splitting technique to treat the negative linear weights when they appear. Table 4.1 indicates that close to fourth-order accuracy can be achieved. For the nonuniform mesh, the measurement of L^∞

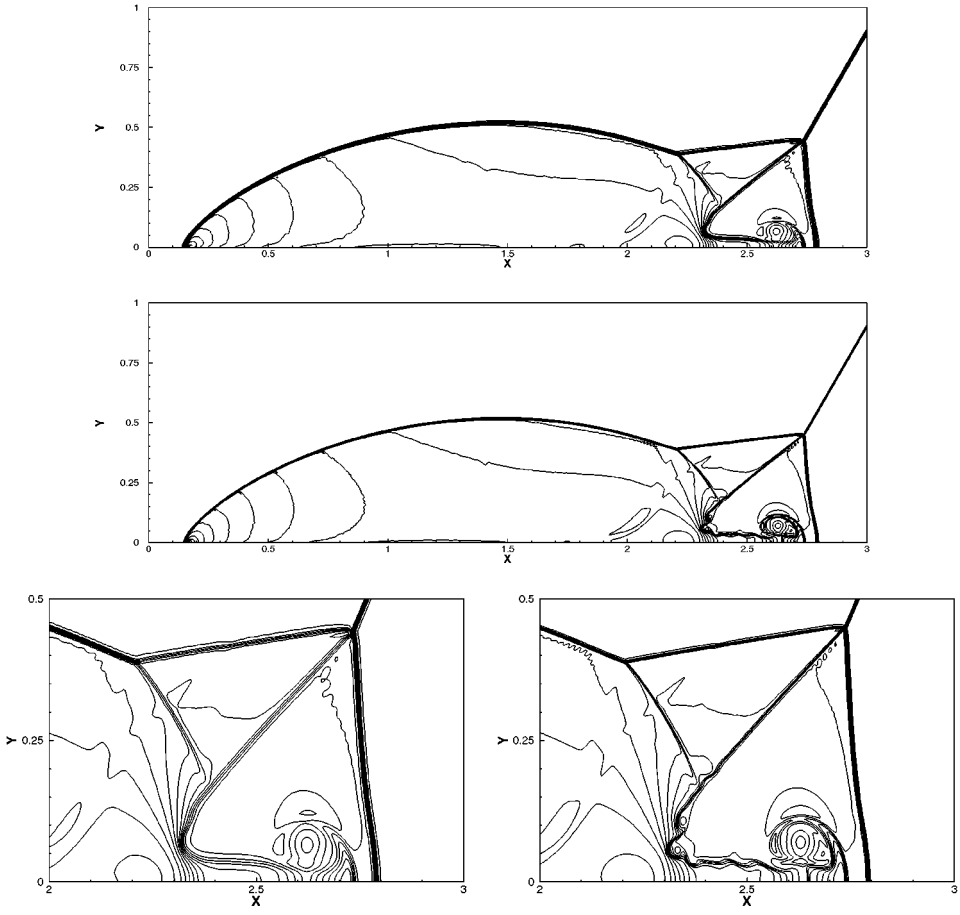

FIG. 3.4. Double Mach reflection, $\Delta x = \Delta y = \frac{1}{240}$ (top and lower left) and $\frac{1}{480}$ (middle and lower right). Dimension by dimension WENO. Blow-up regions at the bottom for details.

errors looks suboptimal, which might be the result of difficulty in defining the order by refinement (the fine mesh is less logically related to the coarse mesh than in the uniform case), and a failure for a cancellation of errors through flux differences as in the uniform mesh case.

TABLE 4.1
2D Burgers Equation: Accuracy Check

Uniform mesh			Nonuniform mesh		
Δx	L^∞ error	Order	Δx	L^∞ error	Order
2.57E-1	6.22E-4		2.67E-1	2.11E-3	
1.29E-1	4.61E-5	3.75	1.26E-1	2.35E-4	2.92
6.43E-2	2.18E-6	4.40	6.32E-2	2.90E-5	3.03
3.21E-2	1.38E-7	3.98	3.34E-2	2.61E-6	3.78
1.61E-2	6.93E-9	4.32	1.66E-2	2.71E-7	3.24
8.08E-3	6.70E-10	3.40	7.44E-3	1.57E-8	3.55

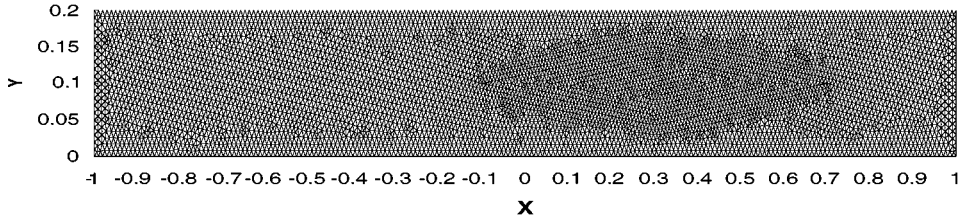

FIG. 4.1. 2D Buckley–Leverett equation: the mesh.

4.2. Discontinuous Problem 1: Scalar Equation in 2D

Having shown the stable results with the splitting treatment of negative linear weights for a fourth-order finite volume WENO scheme for the Burgers equation in Section 2, we now test the fourth-order WENO scheme on the Buckley–Leverett problem whose flux is nonconvex,

$$f(u) = \frac{u^2}{u^2 + 0.25(1-u)^2}, \qquad g(u) = 0,$$

with the initial data $u = 1$ when $-\frac{1}{2} \le x \le 0$ and $u = 0$ elsewhere. The solution is computed up to $t = 0.4$. The exact solution is a shock–rarefaction–contact discontinuity mixture. The mesh we use here is a nonuniform triangulation, shown in Fig. 4.1. Figure 4.2 shows that the waves have been resolved very well.

4.3. Discontinuous Problem 2: System of Equations in 2D

We consider the 2D Euler equations in the domain $[-1, 1] \times [0, 0.2]$. The Sod and Lax shock tube initial data is set in the x-direction, and periodic boundary condition is applied in the y-direction. We use the fourth-order finite volume scheme on triangular meshes to solve the above problem. The mesh we use here is uniform. But we do not seek positive weights as was done in [8], rather we use the splitting technique in Section 2 to treat the

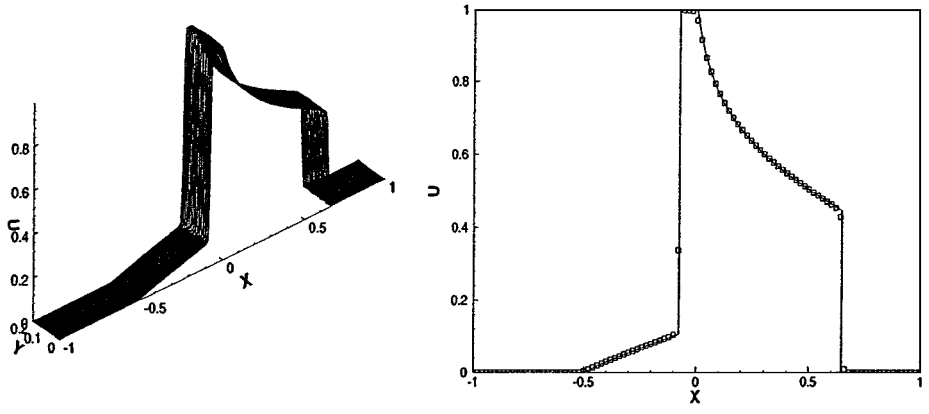

FIG. 4.2. 2D Buckley–Leverett equation at $t = 0.4$, with splitting. Left: the solution surface; Right: the cut at $y = 0.1$ (solid line. exact solution, symbols: numerical solution).

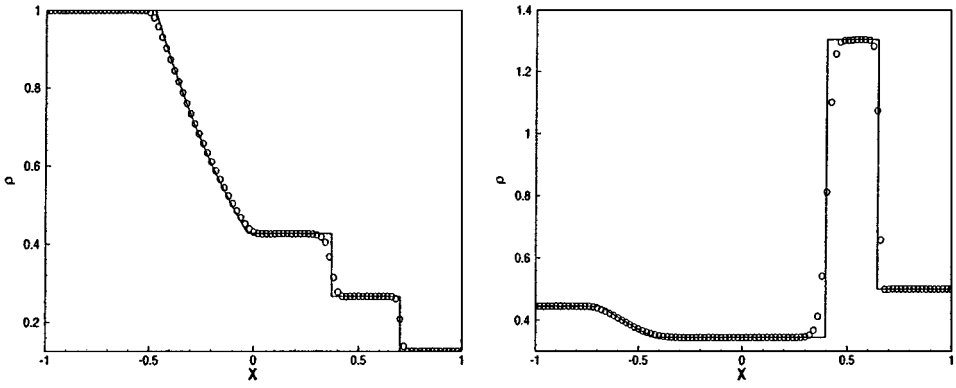

FIG. 4.3. Density plot, Left: Sod problem, Right: Lax problem, with splitting. Roughly 100 points in the x-direction.

negative linear weights when they appear. In fact, we set deliberately certain linear weights to be negative to test the splitting technique. Figure 4.3 shows the numerical results of the Sod and Lax problems.

It seems that there are still oscillations and instability for some nonuniform triangular meshes for the fourth-order WENO schemes applied to Euler equations. For example, the double Mach reflection problem with a highly nonuniform mesh would become unstable at some cells near the shock front. As the method works well for the same meshes with a scalar equation, the problem might be from the characteristic decompositions. When we print out the nonlinear positive and negative weights in the cells immediately before the solution becomes unstable, we found out that, although they stay nicely bounded, they are somewhat "misaligned" so the effect of their difference may put a monotone profile into a nonmonotone one. This could be explained by a hypothetical example of a transition from 1 to 0. Suppose we rewrite this as a difference of a positive group which is a transition from 2 to 0, and a negative group which is from 1 to 0. Suppose also that there is only one transition point in each group. Suppose the positive group has the transition 2, 0.1, 0, and the negative group has the transition 1, 0.9, 0, then each of them is a nice monotone transition but their transition point is misaligned, hence their difference is a transition $1, -0.8, 0$, which has a huge undershoot. In most cases, such misalignments are rare in WENO schemes because both the positive and the negative nonlinear weights are obtained with the same smoothness indicator. However, it seems that for some of the triangular mesh system cases such misalignment does occur. We are still investigating possible remedies for this problem.

5. CONCLUDING REMARKS

We have devised and tested a simple splitting technique to treat the negative linear weights in WENO schemes. This technique involves very little additional CPU time and gives good results in most numerical tests. The only case in which it still yields oscillations and instability is when a fourth-order finite volume WENO method is used on some nonuniform triangular meshes for Euler equations, the reason of which, presumably related to characteristic decompositions, is still under investigation.

REFERENCES

1. D. Balsara and C.-W. Shu, Monotonicity preserving weighted essentially non-oscillatory schemes with increasingly high order of accuracy, *J. Comput. Phys.* **160**, 405 (2000).
2. J. Casper, C.-W. Shu, and H. L. Atkins, Comparison of two formulations for high-order accurate essentially nonoscillatory schemes, *AIAA J.* **32**, 1970 (1994).
3. L. Del Zanna, M. Velli, and P. Londrillo, Dynamical response of a stellar atmosphere to pressure perturbations: numerical simulations, *Astron. Astrophys.* **330**, L13 (1998).
4. O. Friedrichs, Weighted essentially non-oscillatory schemes for the interpolation of mean values on unstructured grids, *J. Comput. Phys.* **144**, 194 (1998).
5. F. Grasso and S. Pirozzoli, Shock-wave-vortex interactions: Shock and vortex deformations, and sound production, *Theor. Comput. Fluid Dyn.* **13**, 421 (2000).
6. F. Grasso and S. Pirozzoli, Shock wave-thermal inhomogeneity interactions: Analysis and numerical simulations of sound generation, *Phys. Fluids* **12**, 205 (2000).
7. A. Harten, B. Engquist, S. Osher, and S. Chakravarthy, Uniformly high order essentially non-oscillatory schemes, III, *J. Comput. Phys.* **71**, 231 (1987).
8. C. Hu and C.-W. Shu, Weighted essentially non-oscillatory schemes on triangular meshes, *J. Comput. Phys.* **150**, 97 (1999).
9. G. Jiang and D.-P. Peng, Weighted ENO schemes for Hamilton–Jacobi equations, *SIAM J. Sci. Comput.* **21**, 2126 (2000).
10. G. Jiang and C.-W. Shu, Efficient implementation of weighted ENO schemes, *J. Comput. Phys.* **126**, 202 (1996).
11. G. Jiang and C.-C. Wu, A high order WENO finite difference scheme for the equations of ideal magnetohydrodynamics, *J. Comput. Phys.* **150**, 561 (1999).
12. D. Levy, G. Puppo, and G. Russo, Central WENO schemes for hyperbolic systems of conservation laws, *Math. Modelling Numer. Anal. (M^2 AN)* **33**, 547 (1999).
13. D. Levy, G. Puppo, and G. Russo, Compact central WENO schemes for multidimensional conservation laws, *SIAM J. Sci. Comput.* **22**, 656 (2000).
14. D. Levy, G. Puppo, and G. Russo, A third order central WENO scheme for 2D conservation laws, *Appl. Numer. Math.* **33**, 415 (2000).
15. S. Liang and H. Chen, Numerical simulation of underwater blast-wave focusing using a high-order scheme, *AIAA J.* **37**, 1010 (1999).
16. R. Liska and B. Wendroff, Composite schemes for conservation laws, *SIAM J. Numer. Anal.* **35**, 2250 (1998).
17. R. Liska and B. Wendroff, Two-dimensional shallow water equations by composite schemes, *Int. J. Numer. Meth. Fluids.* **30**, 461 (1999).
18. X.-D. Liu and S. Osher, Convex ENO high order multi-dimensional schemes without field-by-field decomposition or staggered grids, *J. Comput. Phys.* **142**, 304 (1998).
19. X.-D. Liu, S. Osher, and T. Chan, Weighted essentially non-oscillatory schemes, *J. Comput. Phys.* **115**, 200 (1994).
20. P. Montarnal and C.-W. Shu, Real gas computation using an energy relaxation method and high order WENO schemes, *J. Comput. Phys.* **148**, 59 (1999).
21. S. Noelle, The MoT-ICE: a new high-resolution wave-propagation algorithm for multi-dimensional systems of conservation laws based on Fey's method of transport, *J. Comput. Phys.* **164**, 283 (2000).
22. C.-W. Shu, Essentially non-oscillatory and weighted essentially non-oscillatory schemes for hyperbolic conservation laws, in *Advanced Numerical Approximation of Nonlinear Hyperbolic Equations*, edited by B. Cockburn, C. Johnson, C.-W. Shu, and E. Tadmor, Lecture Notes in Mathematics, (Springer-Verlag, Berlin/New York, 1998), pp. 325–432.
23. C.-W. Shu, High order ENO and WENO schemes for computational fluid dynamics, in High-Order Methods for Computational Physics, edited by T. J. Barth and H. Deconinck, Lecture Notes in Computational Science and Engineering, (Springer-Verlag, Berlin/New York ,1999), Vol. 9, pp. 439–582.

24. C.-W. Shu and S. Osher, Efficient implementation of essentially non-oscillatory shock capturing schemes, *J. Comput. Phys.* **77**, 439 (1988).

25. C.-W. Shu and S. Osher, Efficient implementation of essentially non-oscillatory shock capturing schemes, II, *J. Comput. Phys.* **83**, 32 (1989).

26. P. Woodward and P. Colella, The numerical simulation of two-dimensional fluid flow with strong shocks, *J. Comput. Phys.* **54**, 115 (1984).

27. J. Yang, S. Yang, Y. Chen, and C. Hsu, Implicit weighted ENO schemes for the three-dimensional incompressible Navier–Stokes equations, *J. Comput. Phys.* **146**, 464 (1998).